QUANTIFYING SOURCE EXCITATION AND PATH EFFECTS FOR HIGH-FREQUENCY REGIONAL WAVES

Ru-Shan Wu, Xiao-Bi Xie, Xianyun Wu and Thorne Lay

University of California, Santa Cruz

Sponsored by Defense Threat Reduction Agency

Contract No. DTRA01-01-C-0076

ABSTRACT

The current year study covers two main research directions: Lg wave excitation by explosion sources and Lg wave attenuation and blockage.

Investigation of the excitation of Lg waves by explosions is essential for both understanding Lg wave energy attenuation and for discriminating explosions and earthquakes. Two-dimensional finite-difference calculation and the slowness analysis technique are used to investigate Rg-Lg coupling as an Lg wave excitation mechanism. The method allows us to investigate Lg wave excitation and propagation not only in the space domain, but also in wave number domain. The advantage of the slowness analysis is that it can be applied at close range, before Lg is formed at large distances. This feature is especially useful for the finite-difference approach. Shallow heterogeneous layers are introduced to generate the coupling between the Rg and Lg waves. Heterogeneity models with different scales, different root-mean-square (rms) values, located either near the source or along the entire path, are tested. Their contributions to Lg wave formation are analyzed in the space, slowness and frequency domains.

The half-space screen method developed in the previous project can be used to model Lg wave propagation in complex wave guides including irregular topography, large-scale geological structures and small-scale random heterogeneities. Compared with finite-difference and boundary-element methods, the screen method is very efficient in both computation speed and memory requirements. It is especially useful for Lg wave simulations for high frequencies and regional distances. In this study, anelasticity has been introduced into the screen propagators to handle the effects of intrinsic attenuation for regional Lg. Both P-wave quality factor Q_P and S-wave quality factor Q_S are incorporated into SH wave and P-SV wave calculations. Different attenuation mechanisms including intrinsic attenuation, leakage due to rough topography and Moho discontinuity, and scattering due to small-scale random heterogeneities are simulated and investigated separately. Then, their combined effects on Lg wave propagation in near-realistic crustal wave guides are evaluated and the corresponding apparent Lg quality factors Q_{LG} are calculated.

OBJECTIVE

Introduction

The regional seismic phase Lg is one of the most useful phases for event discrimination and magnitude estimation associated with nuclear explosion and treaty monitoring. The characteristics of Lg are strongly affected by the excitation conditions in the source region and by path effects controlled by waveguide structures of different scales. To obtain a comprehensive understanding of Lg signals, it is crucial to do research on both the excitation and propagation of Lg for realistic crustal models. The Regional Wave Synthetic Seismogram Program in the IGPP branch at the University of California, Santa Cruz, has done extensive work on the excitation and propagation of regional phases, and has developed theory and methods for the investigation of these problems.

A new slowness analysis method allows us to investigate Lg wave excitation in the slowness domain (Xie and Lay, 1994). The main advantage of this method is that it can be applied at close range, before Lg is formed at large distances. This allows us to include fine structure into the model and to study their effects on the Pg to Lg and Rg to Lg coupling. A highly efficient Lg propagation algorithm based on the GSP (Generalized Screen Propagators) method has been developed (Wu et al., 2000) which can propagate high-frequency waves (up to 25 Hz) to long distance (> 1000 km) using a workstation. Wu *et al* (1999) and Wu and Wu (2001) extended the screen method to handle topographic effects by performing conformal or non-conformal transforms. Wu *et al* (2000) extended P-SV screen propagators for Lg simulation by incorporating plane wave reflection coefficients into the screen method. In this paper we report new progress in the following aspects: Rg to Lg scattering as an excitation mechanism for explosion Lg-wave, and simulation of Lg wave attenuation and blockage for complicated crustal waveguide models.

RESEARCH ACCOMPLISHED

Lg-Wave Excitation Through Near Source Rg-Lg Coupling

Lg predominantly comprises shear wave energy trapped in the crust. Explosion sources are expected to be less efficient for excitation of Lg phases than earthquakes to the extent that the source can be approximated as isotropic. Shallow explosions generate relatively large Rg phases compared to deeper earthquakes, and Rg is readily disrupted by crustal heterogeneity. Rg energy may thus scatter into trapped crustal S-waves near the source region and contribute to low-frequency Lg wave (Gupta et al., 1991, 1992). In this study, finite-difference simulations are conducted to generate synthetic seismograms at near regional distance. Random velocity patches are added to the layered crustal model to provide coupling between the Rg and Lg waves. Slowness analysis (Xie and Lay, 1994) is used to investigate the coupling between Rg and Lg, as well as between Pg and Lg, as the excitation mechanisms for explosion generated Lg.

We use a layered velocity structure that resembles East Kazakh crust as the background model. This is a typical high velocity crust with its upper crust P-wave velocity larger than the upper mantle S-wave velocity. For such a velocity structure, very little energy generated from an explosion source can be trapped in the waveguide to form the Lg-wave. To investigate the near source Rg to Lg coupling as the Lg excitation candidate, we add some small random velocity patches near the source region. These random patches are 10 km wide, 2.5 km thick, located at epicentral distance 5-15 km and at different depths. The rms velocity fluctuation for these patches is 20 % with a 1 km correlation length for both vertical and horizontal directions. Figure 1 shows the near source velocity structure with several random velocity patches for different numerical experiments.

The explosion source is located at a depth of 500 m. A Gaussian derivative source time function is used for calculating the synthetic seismograms. The effective frequency band is roughly 0 to 6 Hz. Synthetic seismograms are collected from two receiver arrays for different investigations. The first is a 50x40 array with 0.5 km spacing located at an epicentral distance of 50 km. The second is a 50x40 array with 1 km spacing located at an epicentral distance of 150 km. Synthetic seismograms are generated using a 2D elastic finite-difference code (Xie and Lay, 1994).

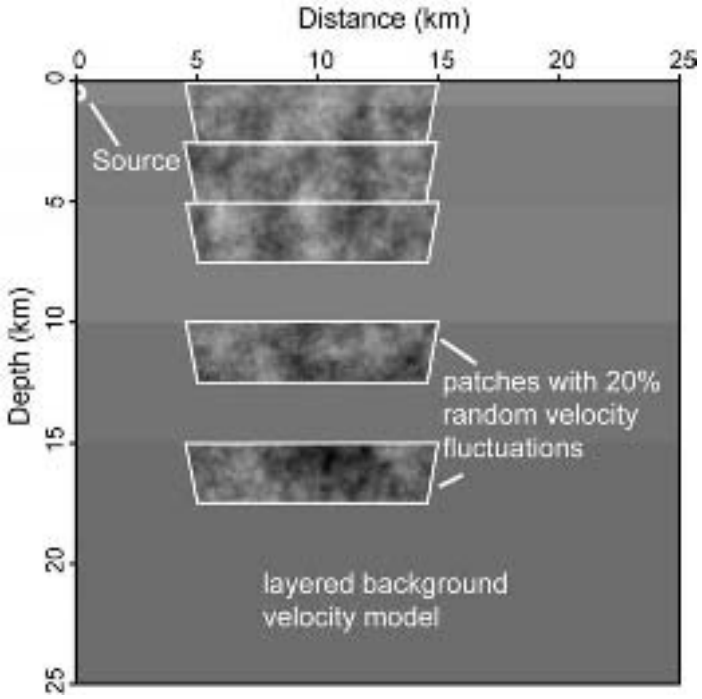

Figure 1. Near source velocity model used for finite-difference simulation. The background velocity is a typical crustal model for East Kazakh. Patches with 20% rms velocity fluctuations are added to the background velocity to generate Pg to Lg scattering and Rg to Lg coupling. These random patches are for different simulations although they are shown here simultaneously.

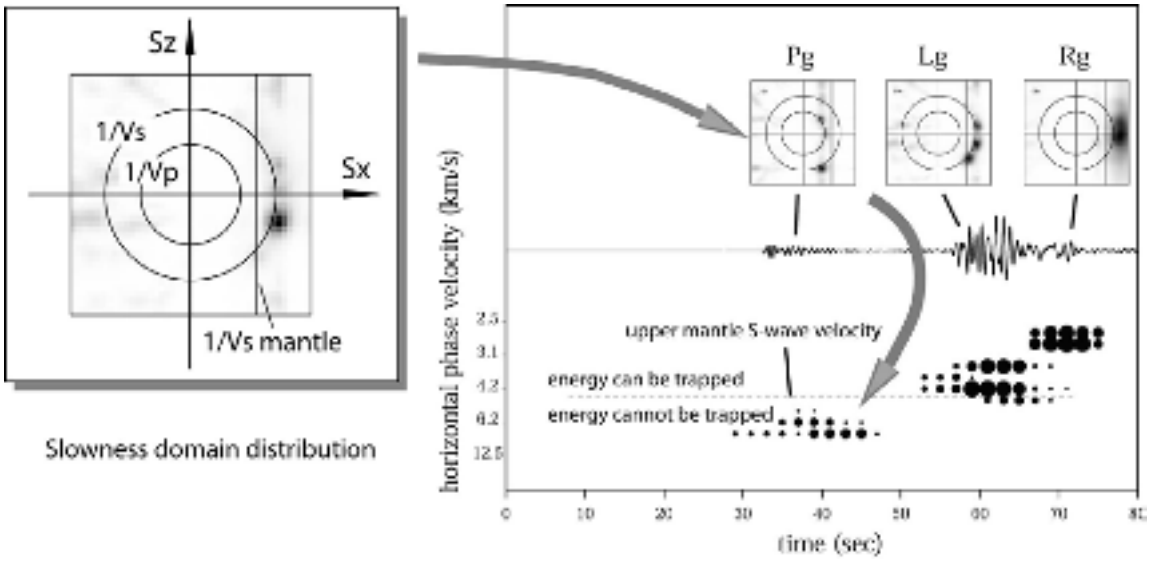

Figure 2. Sketch showing the slowness analysis process.

Synthetic seismograms computed at the receiver arrays are used for the slowness analysis. The size of the sub array for slowness analysis is 10x10. The spacing between the receivers is 0.5 km or 1.0 km, depending on the target wavelengths. Figure 2 is a sketch showing the process of slowness analysis. Shown on the left is the distribution of wave energy in the slowness domain. It is obtained by using a stacking technique and reveals the properties of the propagating waves. Shown in the middle of the right panel is the synthetic seismogram from the center receiver. Shown on the top are energy distributions in the slowness domain for Pg, Lg and Rg group velocity windows. In the Pg window, most energy is P-wave energy and P to S converted wave energy. Since the background model is a

layered crust, the P and S-waves have the same horizontal slowness. In the Lg window, most of the energy is S-wave energy and located on the right side of the upper mantle S-wave velocity (marked with a vertical line). In the Rg window, energy propagates near horizontally and its phase velocities slower than the S-wave velocity. In the lower part of the right panel, the solid circles are energy picked from the slowness domain and stacked from the entire cross section. The size of the circle is proportional to the energy. The vertical axis is apparent horizontal velocity, or equivalently, the reverse horizontal slowness. The dashed line is the upper mantle S-wave velocity. Seismic energy with slowness above this line can be trapped in the crustal waveguide and forms the Lg-wave at larger distance. The energy located below this line cannot be trapped in the crust and will leak to the upper mantle through multiple reflections. It clearly shows the Pg-wave has the lowest slowness; the Rg-wave has the highest slowness, and the Lg-energy is located above the dashed line.

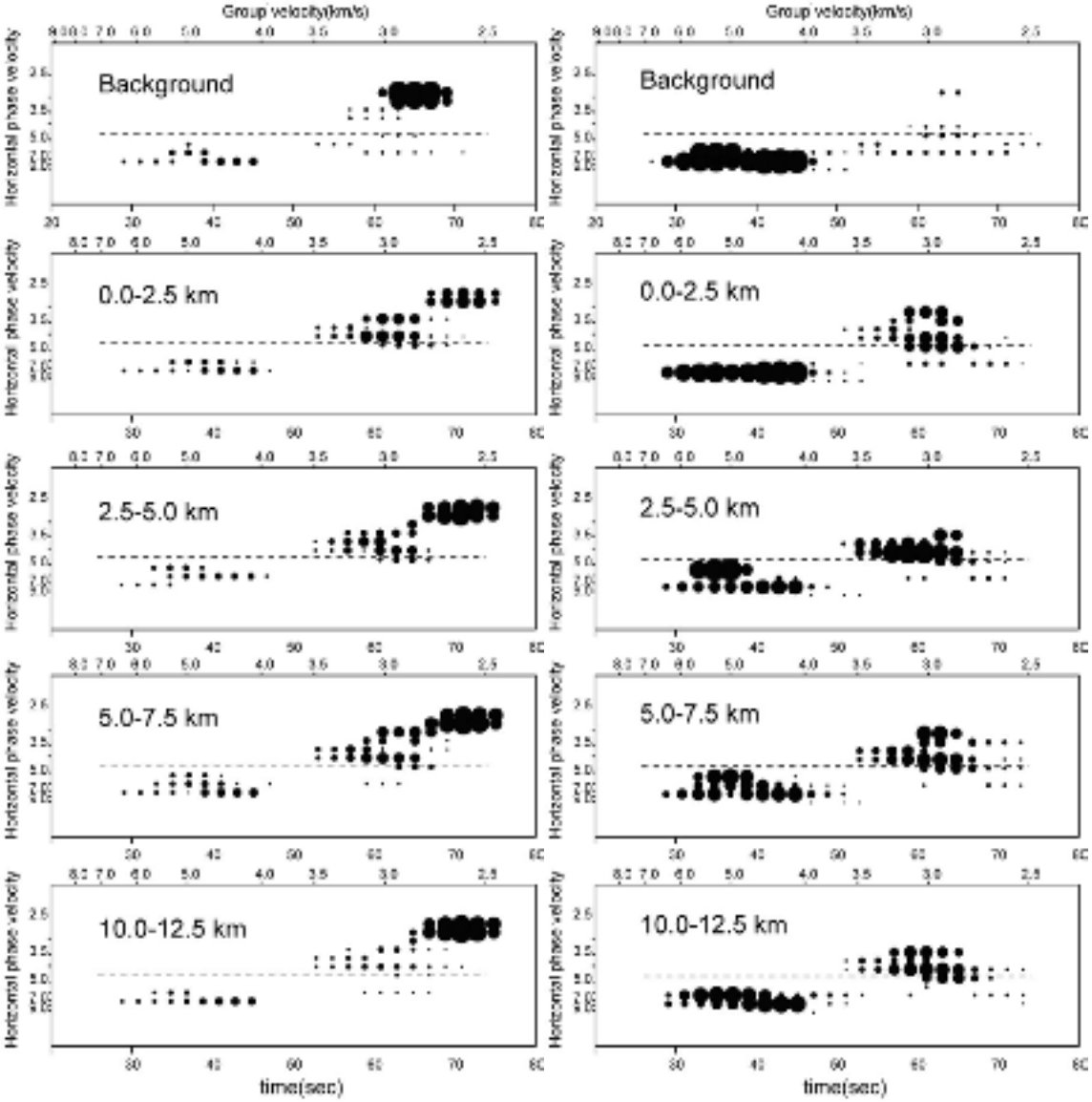

Figure 3. Slowness analysis for velocity models with random patches located at different depths. The left column is for the low-frequency band (0.3-1.5 Hz) and the right column is for the high-frequency band (2.0-5.0 Hz). The top panels are for background velocity model, and the rest of the panels are for random patches at different depths. For details see the text.

To investigate Rg to Lg scattering, a set of random velocity patches are added to the background velocity model. Then, slowness analysis is conducted using synthetic seismograms generated from different models, and for

different frequencies. Figure 3 shows the results for a cross section at 180 km in the crustal waveguide. In each panel, the vertical axis is the horizontal phase velocity. The horizontal axis is time. The group velocity is also marked on the top of each panel. The dashed line marks the upper mantle S-wave velocity. The solid circles are energy picked from the slowness domain and summed up for the entire cross section. The left column is for low frequency (0.3 -1.5 Hz) and the right column is for high-frequency (2.0-5.0 Hz). The top panel is for background velocity model. A dominant feature is that Rg mainly appears as low-frequency signal and Pg mainly appears as high-frequency signal. We first focus on the low-frequency results. From the top panel we can see some Pg-wave and strong fundamental mode Rg-wave. However, such a high velocity crust generate very poor Lg-wave. Within the Lg wave window, only very weak energy can be observed which may be generated by the S*-wave. In the second panel, a random velocity patch located at depth 0.0-2.5 km is added to the background model (refer to Figure 1). Compared with the background model, considerable energy is transferred from the Rg-wave to the Lg-wave through scattering. Panels 3 to 5 are similar to panel 2, except random patches are located at depths 2.5-5.0 km, 5.0-7.5 km and 10.0-12.5 km, respectively. Similar to the case in the second panel, energy is transferred from Rg-wave to Lg-wave. The tendency is: the shallower the random patch the more energy is transferred from Rg to Lg. This also provides additional evidence that the low-frequency Lg energy is coming from the Rg-wave, since the Rg energy is mostly concentrated at shallow depth.

Figure 4 gives the relationship between the depth of the random patch and the low-frequency Rg to Lg scattering. The horizontal axis is the depth of random patches. The upper panel shows the normalized Lg energy, which has the maximum value for the shallowest random patch. With increase of the depth of the random patch, Lg energy decreases toward its background value. The second panel is for normalized Rg energy. It has the lowest energy for the shallowest random patch. With the increase of the depth of the random patch, the Rg energy recovers to its background value. The bottom panel shows the Lg to Rg energy ratio. Its tendency shows the Rg to Lg coupling becoming weaker with increase of the depth of the random patches, which is consistent with the Rg energy distribution in the shallow crust.

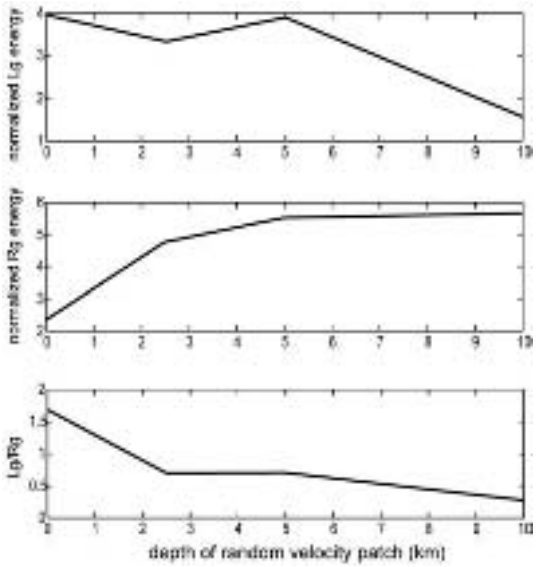

Figure 4. Comparison of normalized energy of Lg and Rg-waves for models with their random velocity patches at different depths.

The right column in Figure 3 is for high-frequency band. From the top panel (background velocity model), we see that the Rg-wave falls outside of this frequency band, and Pg-wave is very strong since it is mainly composed of high-frequency energy. When we add random patches into the background model, considerable high-frequency Lg-wave is generated from the near source scattering of Pg-wave. The strength of the Pg generated Lg-wave does not show strong variation with the depth of the random patches. The numerical simulation and slowness analysis show that near source heterogeneity is responsible for both Rg-Lg coupling and the Pg-Lg scattering. The former contribute to the low-frequency Lg-wave, and the later contribute to the high-frequency energy. The energy partitioning may depends on properties of the source and near source structure.

Simulation of Lg Wave Propagation and Blockage Using Screen Method

Many observed data have shown that regional Lg phase attenuation is related to many factors such as laterally heterogeneous velocity structure, changes in crustal discontinuities, crustal thickness, topographic features, anelastic attenuation, etc. However, the mechanism of Lg wave attenuation has not fully been understood, especially for tectonically active regions that have abnormally low Lg Q. For example in the eastern Tibetan Plateau 1 Hz Lg Q is about 126 (Xie, 2002); and it is about 200 – 267 in various regions of the western United States (Xie and Mitchell, 1990; Xie, 1998), prior numerical simulation results tend to under predict Lg attenuation or blockage. This can be attributed to two reasons. On one hand, realistic crustal models are quite complex so that the parameterized models could be poor approximations. On the other hand, the existing simulation approaches may not have the capacity to handle the effects of the various factors mentioned above.

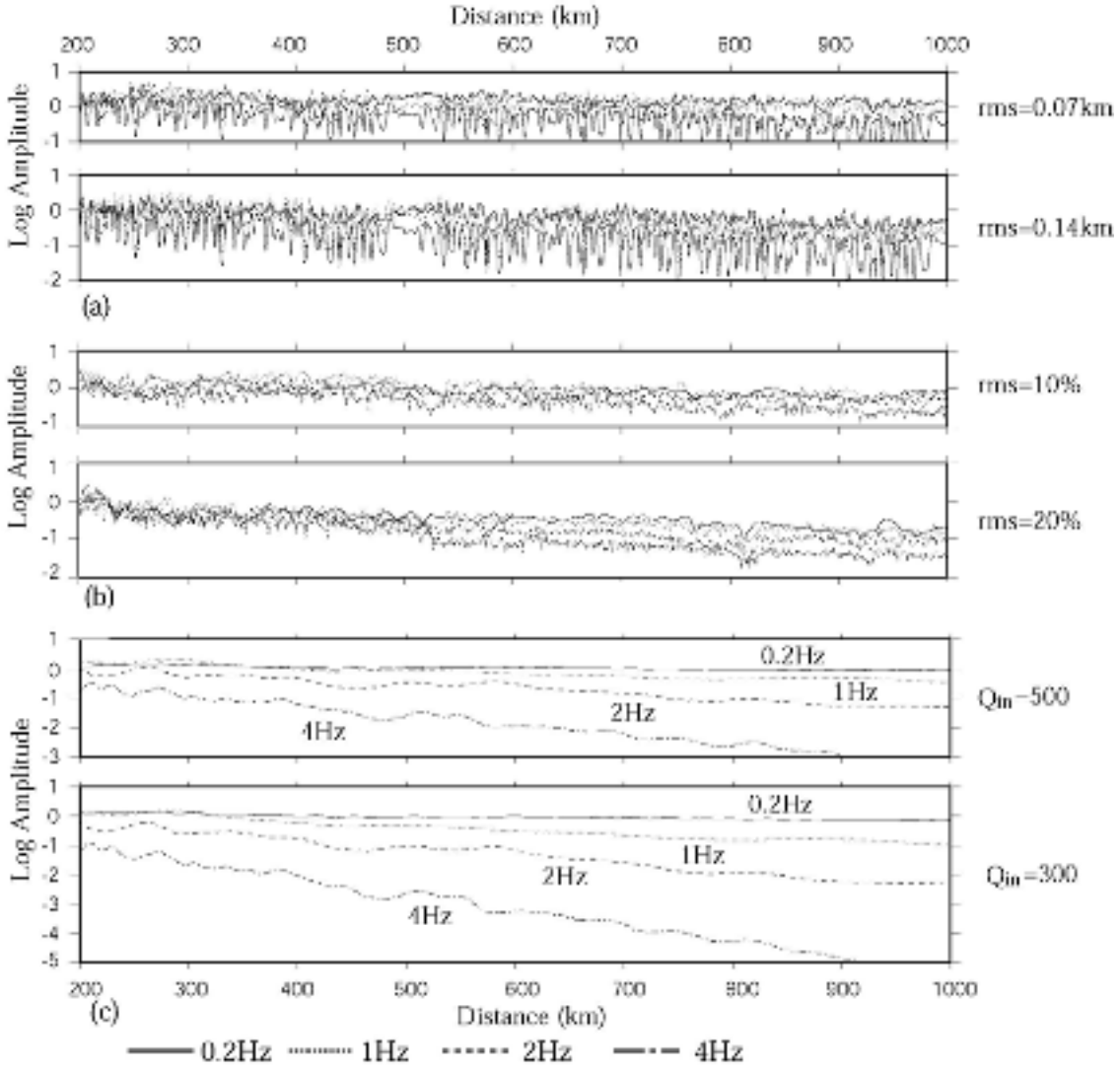

Figure 5 Lg spectral amplitudes at four different frequencies versus distance for crustal models with topographies only (a), crustal heterogeneities only (b), and intrinsic attenuation only (c). Topography with rms=0.07km has a fluctuation of 0.87~-0.75km in height. Q_{in} denotes quality factor of shear wave.

In this section, using the screen method incorporated with anelastic quality factor Q_{in}, Lg wave simulations including the effects of random topographies, crustal heterogeneities and anelastic attenuation are conduced,

separately. We estimate apparent Lg Q and its power-law frequency dependence associated with different attenuation mechanisms. Then, we synthesize Lg wave responses to a real crustal geometry in the Tibetan Plateau, assuming different heterogeneities and intrinsic attenuations. Preliminary simulation results reveal high Lg attenuation or blockage after introducing low Q_{in} (intrinsic quality factor of shear wave) into the model.

A. Scattering, anelasticity, and Lg Q

The crustal model for simulations consists of a crustal layer and a half-space mantle. The parameters of the crust and mantle are $V_{crust} = 3.5km/s$, $\rho_{crust} = 2.8g/cm^3$, $V_{mantle} = 4.5km/s$, and $\rho_{mantle} = 3.1g/cm^3$. The thickness of the crust is 32km. Two random topographies used have the same correlation length of 2.5 km but different rms fluctuations: rms=0.07km (height: 0.87~-0.75km) and rms=0.14km (height: 1.75~-1.5km). A random medium with an exponential correlation function is used to model crustal heterogeneity. Its correlation lengths are 10 km in range and 5 km in depth. The rms values used are 10% and 20%, respectively. A source is located at a depth of 8 km and has a spectrum function given by:

$$S(f) = \frac{1}{1 + (f / f_c)^2}$$

where f is frequency and $f_c = 2Hz$ is the dominant frequency. For the screen method computation, the step length for each forward step is 125 m. The spatial sampling in depth is 250 m. The number of samples in depth is 512. The number of screens is 8000 corresponding to a regional distance of 1000km. We calculate 6 sets of Lg synthetic seismograms for different crustal models. Figure 5 shows spectral amplitudes versus distance for four different frequencies: 0.2, 1., 2., and 4Hz. Figure 5a involves the scattering effect of irregular surface only. Fluctuation of Lg spectral amplitudes versus distance increases as frequency and/or topographies increase, while the averaged spectral amplitudes show a weak attenuation for either low or high frequencies. Figure 5b involves the scattering effect of heterogeneities only. Fluctuation of Lg spectral amplitudes is weak compared with those in Figure 5a. Figures 5a and b show that although topographies and crustal heterogeneities may directly affect Lg wave behavior, they cannot fully account for high Lg attenuation or blockage. Figure 5c involves only the effect of anelastic attenuation. We see that Lg spectral amplitudes vary smoothly with distance, and high-frequency Lg waves shows strong attenuation.

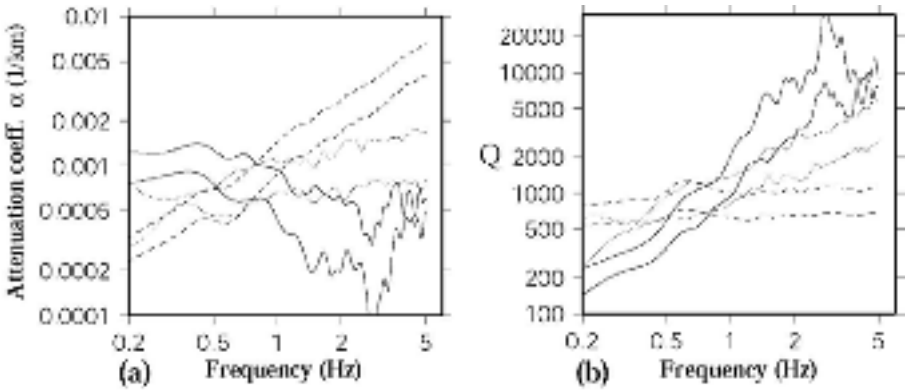

Figure 6. (a) Attenuation coefficient versus frequency, (b) Apparent Lg Q versus frequency. Solid lines correspond to the models with random topographies, dotted lines to models with random heterogeneities, and dashed lines to the anelastic crustal wave guides.

Assume that in 2-D, the Lg spectral amplitude can be expressed by:

$$A_{Lg}(f) = S(f)e^{-\frac{\pi f}{Q}\frac{x}{v}} = s(f)e^{-\alpha x}$$

where α is attenuation coefficient, x propagation distance, v Lg group velocity, and Q is apparent Lg Q being frequency-dependent. Then we can calculate attenuation coefficient and Lg Q by linearly fitting Lg spectral amplitudes shown in Figure 5. Figure 6 shows the estimated attenuation coefficients and apparent Lg Q's versus frequency. Solid lines correspond to the models with random topographies, dotted lines to the models with random heterogeneities, and dashed lines to anelastic crustal wave guides. We see that apparent Lg Q's show different frequency-dependent relations for different attenuation mechanisms.

The Lg Q has often been observed to fit a power-law frequency dependence as:

$$Q_{Lg}(f) = Q_0 f^{\eta}$$

where Q_0 and η are Lg Q at 1 Hz and its power-law frequency dependence. Using the above relation and Figure 6b, we can estimate Q_0 and η (listed in Table 1). From Table 1 we see that the Lg frequency dependence η for homogeneous anelastic crusts is much smaller than those ($0.3 < \eta < 0.6$) for most practical earthquakes and explosions, while the η associated with scattering by random topographies or random heterogeneities varies strongly. It may be possible to generate appropriate η by combining intrinsic attenuation and the attenuation due to scattering.

Table 1. Estimated Q_0 and η

	Topography		Heterogeneity		Intrinsic Q_{in}	
	D*=0.07km	D=0.14km	B**=10%	B=20%	500	300
Q_0	2029	945	1345	827	508	313
η	2.320	1.700	0.888	0.73	0.057	0.056

*D denotes the rms for random topography and B** denotes the rms for random medium.

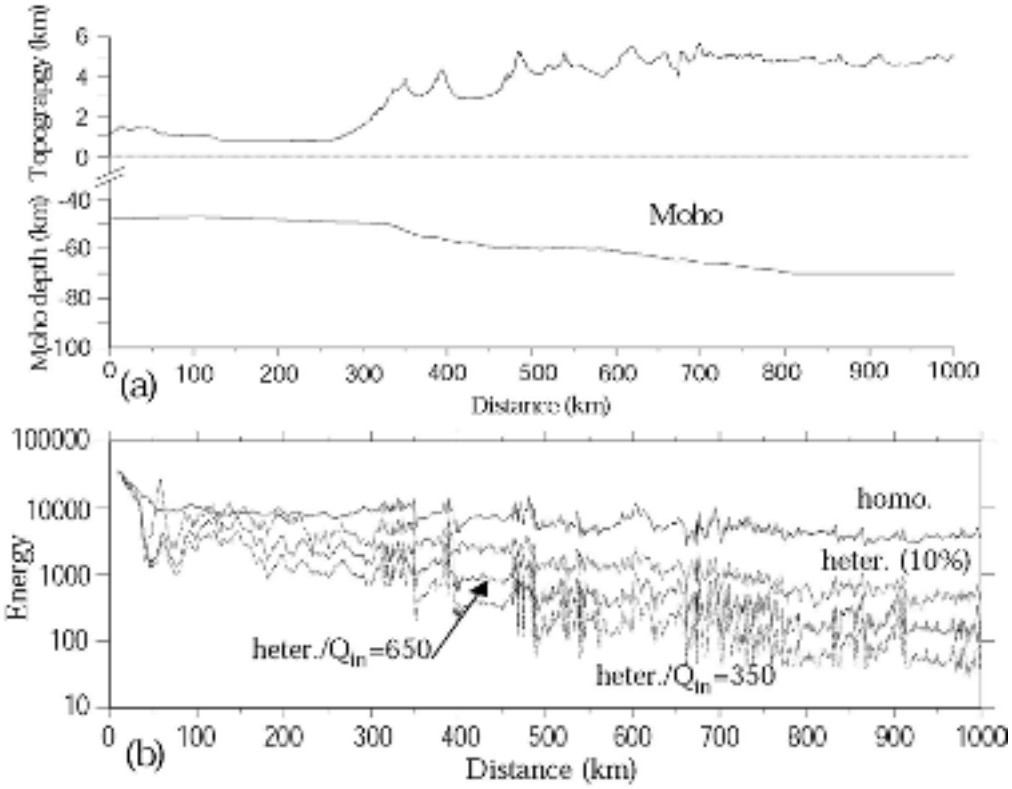

Figure 7 (a) A cross-section profile of a real crust in the Tibetan Plateau (a segment of the crust given in Fan and Lay, 1998). (b) Lg wave energy versus distance for the crustal model with different heterogeneities and anelastic attenuations. Solid line corresponds to a homogeneous elastic waveguide, dashed line to the crust with rms=10% heterogeneities, and dotted and dotted-dashed lines to the crusts with different intrinsic attenuation Q_{in}: 500 and 300, in addition to rms=10% heterogeneities.

B. Lg wave simulation with real crustal wave guides

Although the propagation of Lg has been observed across most of Asia, Lg has not been observed for paths crossing the Tibetan Plateau. It has been demonstrated that Lg has abnormally strong attenuation in these regions. Figure 7a shows a cross-section profile of a real crust in the Tibetan Plateau (Part segment of the crust given in Fan and Lay, 1998). This crust has severe topography and great changes in lateral velocity structure. Also we will introduce certain heterogeneities and anelastic attenuation into the crustal model to investigate the mechanism of Lg attenuation or blockage. Topography data have a resolution of 1 km in range and Moho depth data have a resolution of 10 km in range. For numerical computation using the screen method, both data sets are linearly interpolated up to a sampling interval of 0.125 km. Other parameters are the same as used in Figure 5. We first synthesize full seismograms for regional distances up to 1000 km and calculate Lg wave energy (excluding Sn) by summing up the energy of all frequency components of Lg waves for each receiver. Figure 7b shows Lg wave energy versus distance for the crusts with rms=10% heterogeneities and different anelastic attenuations. The solid line corresponds to an elastic homogeneous waveguide. Lg energy fluctuation is closely related to topography but Lg energy attenuation is weak in the whole range. Even at the distance of 1000 km, high-frequency Lg phase is still strong (see Figure 8b). The dashed line corresponds to the crust with rms=10% heterogeneities; the dotted and dotted-dashed lines to the crusts with different intrinsic attenuation Q_{in}: 500 and 300, as well as rms=10% heterogeneities. We see that after introducing anelastic attenuation, Lg waves show high attenuation. Note that Lg energy for the crust with Q_{in} =300 at far receivers (> 600 km), mainly comes from low-frequency Lg waves (see Figure 8a).

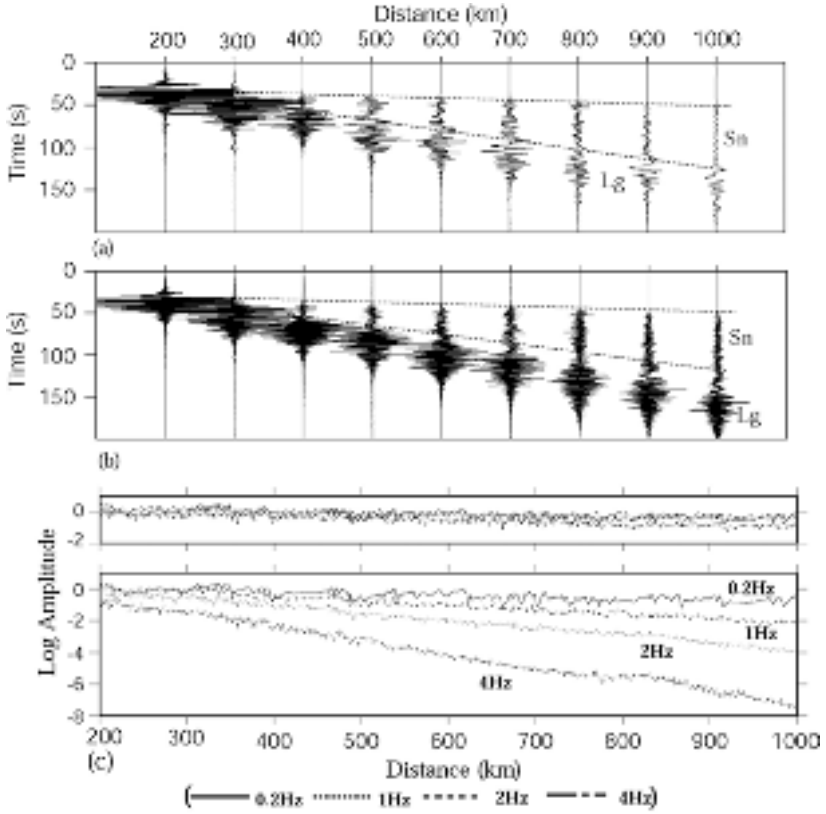

Figure 8 (a) Synthetic seismograms for the crust with variable anelastic attenuation along the path, (b) synthetic seismograms for the elastic crust with rms=10% heterogeneities, and (c) Lg spectral amplitudes versus distance at 4 different frequencies calculated from (a) and (b), respectively.

Another example is that, assuming anelastic attenuation to be variable along the path, we let Q_{in} be 450 for a range below 300 km, 250 for a range between 300 – 800 km, and 125 for a range greater than 800 km. Corresponding synthetic seismograms are shown in Figure 8a. The time axis is reduced by a velocity of 6 km/s. We see that high-frequency Lg waves are weak at the distance of 800 km, and absent at 1000 km. For comparison, synthetic seismograms for an elastic heterogeneous waveguide are given in Figure 8b. High-frequency Lg waves are very

strong at far receivers up to 1000 km. Figure 8c shows Lg spectral amplitudes at four different frequencies versus distance calculated from Figures 8a and b. We see that the slope of high-frequency Lg spectral amplitudes varies for different segments of the path.

CONCLUSIONS AND RECOMMENDATIONS

In conclusion, the existence of near source heterogeneities provides coupling between the Rg- and Lg-waves, as well as Pg- and Lg-waves. The numerical simulation and slowness analysis show that the near source scattering of fundamental mode Rg-wave can generate low-frequency Lg-wave. This is consistent with the previous observation from real data. The near source heterogeneities can also cause the scattering of high-frequency Pg-wave and contribute to the high-frequency Lg-wave. However, the low- and high-frequency Lg waves may have different attenuation patterns in their later propagation stage. Combining the excitation and propagation investigations together will give a complete description for Lg-wave.

Apparent Lg Q produced by intrinsic attenuation and scattering due to topography and random heterogeneities, shows different frequency dependence. Intrinsic attenuation shows a quite small apparent η (nearly constant Q), while scattering due to topography and heterogeneities may generate large η. Either intrinsic attenuation or scattering attenuation alone cannot satisfactorily explain the observed frequency dependence of apparent Lg Q. A combination of different attenuation mechanisms may be required. Lg wave simulation for a real crust in the Tibetan Plateau shows that anelastic attenuation, combined with scattering by heterogeneities may cause high Lg attenuation even blockage.

REFERENCES

Fan G. and T. Lay (1998), Statistical analysis of irregular wave-guide influences on regional seismic discriminants in China: Additional results for P_n / S_n, P_n / Lg, and P_g / S_n, *Bull. Seis. Soc. Am.* **88** (6), 1504-1510.

Gupta, I.N., W.W. Chan, and R.A. Wagner (1992), A comparison of regional phases from underground nuclear explosions at east Kazakh and Nevada test sites, *Bull. Seism. Soc. Am*., **8**2, 352-382.

Gupta, I.N., T.W. McElfresh, and R.A. Wagner (1991), Near source scattering of Rayleigh to P in teleseismic arrivals from Pahute Mesa (NTS) shots, in *Explosion Source Phenomenology*, edited by, Taylor, S.R., Patton, H.J. and Richards, P.G., American Geophysical Union, Washington, DC.

Wu, R.S., S. Jin, X.B. Xie (2000), Seismic wave propagation and scattering in heterogeneous crustal wave guides using screen propagators: I SH waves, *Bull. Seis. Soc. Am*., **90**, 401-413.

Wu, X.Y., and R.S. Wu (2001), Lg-wave simulation in heterogeneous wave guides with surface topography using screen propagators, *Geophys. J. Int*., **146**, 670-678.

Xie, J. (1998), Spectral inversion of Lg from earthquakes: A modified method with application to the 1995, western Texas earthquake sequence, *Bull. Seis. Soc. Am*., **88**, 1525-1537.

Xie, J. (2002), Lg Q in the Eastern Tibetan Plateau, *Bull. Seis. Soc. Am*., **92**, 871-876.

Xie, J., and B.J. Mitchell (1996), Attenuation of multiphase surface waves in the Basin and Range province. I. Lg and Lg Coda, *Geophys. J. Int*., **102**, 121-137.

Xie, X.B. and T. Lay (1994), The excitation of Lg waves by explosions: A finite-difference investigation, *Bull. Seism. Soc. Am*., **84**, 324-342.

Xie, X.B. and T. Lay (1995), The log(rms Lg)-mb scaling law slope, *Bull. Seism. Soc. Am*, **85**, 834-844.